Proceedings of the ECCOMAS Thematic International Conference on Simulation and Modeling of Biological Flows (SIMBIO 2011) September 21–23, 2011, VUB, Brussels, Belgium

Algorithms for the coupling of one-dimensional arterial networks with three-dimensional fluid-structure interaction problems

A. Cristiano I. Malossi[1], Simone Deparis[1], and Pablo J. Blanco[2]

1 CMCS, Chair of Modelling and Scientific Computing, MATHICSE, Mathematics Institute of Computational Science and Engineering, EPFL, École Polytechnique Fédérale de Lausanne, Station 8, CH-1015, Lausanne, Switzerland, e-mails: cristiano.malossi@epfl.ch, simone.deparis@epfl.ch.

2 LNCC, Laboratório Nacional de Computação Científica, Av. Getúlio Vargas 333, Quitandinha, 25651-075, Petrópolis, Brazil, e-mail: pjblanco@lncc.br.

Abstract

This work is focused on the development of a geometrical multiscale framework for modeling the human cardiovascular system. This approach is designed to deal with different geometrical and mathematical models at the same time, without any preliminary hypotheses on the layout of the general multiscale problem. This flexibility allows to set up a complete arterial tree model of the circulatory system, assembling first a network of one-dimensional models, described by non-linear hyperbolic equations, and then replacing some elements with more detailed (and expensive) three-dimensional models, where the Navier–Stokes equations are coupled with structural models through fluid-structure interaction algorithms. The coupling between models of different scale and type is addressed imposing the conservation equations in terms of averaged/integrated quantities (i.e., the flow rate and the normal component of the traction vector); in particular, three coupling strategies have been explored for the fluid problem. In all the cases, these strategies lead to small non-linear interface problems, which are solved using classical iterative algorithms.
Keywords: Geometrical multiscale; Fluid-structure interaction algorithms; Cardiovascular networks; Hemodynamics.

Introduction

The simulation of blood-flow in the human body is a challenging task. A very accurate model should account for the arterial and venous networks, the heart, and the capillaries, keeping into account also the non-Newtonian blood behavior and complex wall constitutive laws. Even with nowadays powerful supercomputers it is not possible to solve such a problem and several approximations must be employed.

A first approximation is to consider reduced models for the fluid-structure interaction (FSI) dynamics [1] and glue them together by the imposition of integrated quantities in an explicit hierarchical fashion [1, 2, 3, 4, 5] or implicitly [6]. The resulting model is a network of one-dimensional (1-D) models for the arterial system, which can be closed with zero-dimensional (0-D) models to account for the left heart ventricle and the capillaries (and therefore neglecting the venous system).

Another possible approximation is to restrict the region of interest and consider a three-dimensional (3-D) fluid-structure simulation. As pointed out in, e.g., [7], in these cases it is important to select appropriate boundary conditions. These can be found either by direct measurements of integral quantities, like flow rates [8, 9], or by using a separate 1-D network to provide the correct boundary data [10]. It is also possible to couple the 1-D network with the 3-D model; in [11, 12] the authors propose an explicit coupling between such models.

In this work we use the methodology described in [13] and we couple these single models in an implicit fashion; then we solve the coupled problem by inexact-Newton iterations on the coupling variables. Each model used in the network has its own *optimal* time discretization step and often this also has an upper bound limitation derived from the CFL condition [1] in the case of explicit algorithms. When discretizing in time the coupling of many models of equal or different scales we shall therefore use the most stringent condition, which may lead to unnecessary computation. Here we propose to use two time step scales, one for the global arterial tree and one for the local 3-D models, the former typically having a smaller time step due to its explicit nature.

Models

In the following paragraphs we briefly introduce the geometrically-heterogeneous models which are the main *ingredients* of our geometrical multiscale framework.

3-D FSI model

In a geometrical multiscale setting, 3-D FSI models are used for modeling components where the geometrical description play a fundamental role, e.g., in vessels with aneurysms, stenoses, or other complex pathologies. In those cases, a 3-D description of the flow field is mandatory in order to capture the true physics of the phenomena.

Equations The blood dynamics of the 3-D FSI model is described by formulating the incompressible Navier–Stokes equations for Newtonian fluids in moving domains. We choose to use an Arbitrary Lagrangian Eulerian (ALE) frame of reference [14].

Let $\Omega = \Omega_\mathrm{f} \cup \Omega_\mathrm{s}$ be a reference configuration of the fluid-structure system, with Ω_f and Ω_s the reference domains for the fluid and the solid, respectively. We denote by $\Gamma_\mathrm{FSI} \stackrel{\mathrm{def}}{=} \partial\Omega_\mathrm{f} \cap \partial\Omega_\mathrm{s}$ the fluid-solid interface. The current configuration of the fluid domain, $\Omega_\mathrm{f}(t)$, is parametrized by the ALE map

$$\begin{aligned} \mathcal{A}_t : \Omega_\mathrm{f} &\to \Omega_\mathrm{f}(t) \\ \mathbf{x} &\mapsto \mathcal{A}_t(\mathbf{x}) = \mathbf{x} + \mathbf{d}_\mathrm{f}(\mathbf{x}), \end{aligned}$$

as $\Omega_\mathrm{f}(t) = \mathcal{A}_t(\Omega_\mathrm{f}, t)$, where $\mathbf{d}_\mathrm{f} : \Omega_\mathrm{f} \times \mathbb{R}^+ \to \mathbb{R}^3$ denotes the displacement of the fluid domain. We denote by $\Gamma_\mathrm{FSI}(t) \stackrel{\mathrm{def}}{=} \partial\Omega_\mathrm{f}(t) \cap \partial\Omega_\mathrm{s}(t)$ the current position of the fluid-solid interface. In practice, $\mathbf{d}_\mathrm{f} = \mathrm{Ext}(\mathbf{d}_\mathrm{s}|_{\Gamma_\mathrm{FSI}})$, where $\mathbf{d}_\mathrm{s} : \Omega_\mathrm{s} \times \mathbb{R}^+ \to \mathbb{R}^3$ stands for the solid displacement and $\mathrm{Ext}(\cdot)$ is an harmonic lifting operator from Γ_FSI to Ω_f.

The nonlinear fluid-structure problem under consideration reads as follows (see e.g. [7, Chapter 11]): find the fluid velocity $\mathbf{u} = \mathbf{u}(\mathbf{x}, t) : \Omega_\mathrm{f} \times \mathbb{R}^+ \to \mathbb{R}^3$, the pressure $p = p(\mathbf{x}, t) : \Omega_\mathrm{f} \times \mathbb{R}^+ \to \mathbb{R}$, and the solid displacement $\mathbf{d}_\mathrm{s} = \mathbf{d}_\mathrm{s}(\mathbf{x}, t) : \Omega_\mathrm{s} \times \mathbb{R}^+ \to \mathbb{R}^3$ such that

$$\begin{cases} \rho_\mathrm{f}\partial_t\mathbf{u}|_\mathcal{A} + \rho_\mathrm{f}(\mathbf{u} - \mathbf{w}) \cdot \nabla\mathbf{u} - \nabla \cdot \boldsymbol{\sigma}_\mathrm{f} = \mathbf{0} & \text{in } \Omega_\mathrm{f}(t), \\ \nabla \cdot \mathbf{u} = 0 & \text{in } \Omega_\mathrm{f}(t), \\ \rho_\mathrm{s}\partial_{tt}\mathbf{d}_\mathrm{s} - \nabla \cdot \boldsymbol{\Pi} = \mathbf{0} & \text{in } \Omega_\mathrm{s}, \end{cases}$$

with the following fluid-structure interface coupling conditions

$$\begin{cases} \mathbf{d}_\mathrm{f} = \mathrm{Ext}(\mathbf{d}_\mathrm{s}|_{\Gamma_\mathrm{FSI}}), \quad \mathbf{w} = \partial_t\mathbf{d}_\mathrm{f} & \text{in } \Omega_\mathrm{f}, \\ \mathbf{u} = \partial_t\mathbf{d}_\mathrm{s} & \text{on } \Gamma_\mathrm{FSI}(t), \\ \boldsymbol{\Pi}\mathbf{n}_\mathrm{s} = -J_\mathrm{f}\boldsymbol{\sigma}_\mathrm{f}(\boldsymbol{F}_\mathrm{f})^{-\mathrm{T}}\mathbf{n}_\mathrm{f} & \text{on } \Gamma_\mathrm{FSI}. \end{cases}$$

The initial conditions are: $\mathbf{u}(0) = \mathbf{0}$, $\mathbf{d}_\mathrm{s}(0) = \mathbf{0}$ and $\partial_t\mathbf{d}_\mathrm{s}(0) = \mathbf{0}$; ρ_f and ρ_s represent the fluid and solid densities, respectively, $\partial_t|_\mathcal{A}$ the ALE time derivative, $\boldsymbol{\sigma}_\mathrm{f} = \boldsymbol{\sigma}_\mathrm{f}(\mathbf{u}, p) \stackrel{\mathrm{def}}{=} -p\mathbf{I} + 2\mu\boldsymbol{\epsilon}(\mathbf{u})$ the fluid Cauchy stress tensor, μ the fluid dynamic viscosity, $\boldsymbol{\epsilon}(\mathbf{u}) \stackrel{\mathrm{def}}{=} 1/2\left(\nabla\mathbf{u} + \nabla\mathbf{u}^\mathrm{T}\right)$ the strain rate tensor, $\boldsymbol{\Pi} = \boldsymbol{\Pi}(\mathbf{d}_\mathrm{s})$ the first Piola–Kirchhoff stress tensor of the structure, $\boldsymbol{F}_\mathrm{f} \stackrel{\mathrm{def}}{=} \nabla\mathcal{A}$ the fluid domain gradient of deformation and $J_\mathrm{f} \stackrel{\mathrm{def}}{=} \det \boldsymbol{F}_\mathrm{f}$ the Jacobian; $\mathbf{n}_\mathrm{f}$ and $\mathbf{n}_\mathrm{s}$ are, respectively, the outward unit normals to the fluid and solid domains.

In the linearized St. Venant–Kirchhoff model the Piola tensor is approximated as

$$\boldsymbol{\Pi} \approx \lambda\mathrm{tr}(\boldsymbol{\epsilon}_\mathrm{s})\mathbf{I} + 2\mu_\mathrm{s}\boldsymbol{\epsilon}_\mathrm{s},$$

with $\boldsymbol{\epsilon}_\mathrm{s} = 1/2\left(\nabla\mathbf{d}_\mathrm{s} + \nabla\mathbf{d}_\mathrm{s}^\mathrm{T}\right)$ and λ and μ_s the two Lamé coefficients.

The harmonic extension problem associated to the operator $\mathrm{Ext}(\cdot)$ reads: find $\mathbf{d}_\mathrm{f} = \mathbf{d}_\mathrm{f}(\mathbf{x}, t) : \Omega_\mathrm{f} \times \mathbb{R}^+ \to \mathbb{R}^3$ such that

$$\begin{cases} -\Delta\mathbf{d}_\mathrm{f} = \mathbf{0}, & \text{in } \Omega_\mathrm{f}, \\ \mathbf{d}_\mathrm{f} = \mathbf{d}_\mathrm{s}, & \text{on } \Gamma_\mathrm{FSI}. \end{cases} \tag{1}$$

The problem is finally closed by imposing a suitable set of boundary conditions on the external wall of the solid Γ_wall and at all the other fluid and solid external interfaces. The later are automatically provided by the adjacent 1-D models within the geometrical multiscale problem (as we see in the forthcoming section), while for the former we postpone the discussion to the section of results.

Numerical approximation For the time discretization of the 3-D FSI problem we use a geometry-convective explicit scheme (GCE) [15], i.e., the convective field and the fluid computational domain are extrapolated from the previous time step. The other terms are treated with a first order backward Euler scheme. The Navier–Stokes equations therefore reduce to the linear Oseen equations, leading to a linear 3-D FSI problem at each time step. The Oseen equations are then discretized in space by a $\mathbb{P}1$–$\mathbb{P}1$ Finite Element (FE) method, stabilized through interior penalty (see [16]), which shows a convergence of order one in h (the spatial discretization of the whole domain Ω_f) for both velocity and pressure.

The structural equations are also linear and require no special treatment. Since the geometry is treated explicitly, the fluid computational domain $\Omega_\mathrm{f}(t^{k+1})$ is computed by using $\mathbf{d}_{\Gamma_\mathrm{s}}^k$ as boundary condition in (1). Thus the coupled 3-D FSI model after discretization gives at each time step t^{k+1} a monolithic linear system to solve for

$$\begin{bmatrix} \mathrm{F_{ff}} & \mathrm{F_{f\Gamma}} & & & \\ \mathrm{F_{\Gamma f}} & \mathrm{F_{\Gamma\Gamma}} & & & \mathrm{I} \\ & & \mathrm{S_{ss}} & \mathrm{S_{s\Gamma}} & \\ & & \mathrm{S_{\Gamma s}} & \mathrm{S_{\Gamma\Gamma}} & -\mathrm{I} \\ & -\mathrm{I} & & \mathrm{I}/\Delta t & \end{bmatrix} \begin{bmatrix} \mathbf{y}^{k+1} \\ \mathbf{y}_\Gamma^{k+1} \\ \mathbf{d}^{k+1} \\ \mathbf{d}_\Gamma^{k+1} \\ \lambda^{k+1} \end{bmatrix} = \begin{bmatrix} \mathbf{f}_\mathrm{f}^{k+1} \\ \mathbf{0} \\ \mathbf{f}_\mathrm{s}^{k+1} \\ \mathbf{0} \\ \mathbf{d}_\Gamma^k/\Delta t \end{bmatrix}, \tag{2}$$

where $\mathbf{y}^k := (\mathbf{u}^k, p^k)$ denotes the fluid variables, vectors with sub-indices Γ represent all the variables on the fluid-structure interface Γ_FSI, λ^k is a Lagrange multiplier that

corresponds to the force transferred from fluid to structure, and the blocks F_{ij} and S_{ij}, $i,j = \mathrm{f},\mathrm{s}$, or Γ correspond to the sub-blocks of the finite element matrices of the fluid and structure problems respectively. The 3-D FSI system (2) is solved by a GMRES method preconditioned by overlapping algebraic Schwarz preconditioners based on an inexact block factorization of the system in the block-composed form. The solution strategy of the monolithic 3-D FSI system (2) is detailed in [15].

1-D model

The global arterial circulation can be modeled by a network of 1-D elements, each one characterized by a circular cross-section (eventually narrowed along the axial direction) and a viscoelastic arterial wall (see, for instance, [1, 3, 5]). Even if the 1-D model is very simple and does not account for the 3-D geometrical description of the vessels, it has been proven to be able to accurately capture the behaviour of the principal physiological quantities, like the volumetric flow rate and the mean pressure. For this reason, in a geometrical multiscale setting, the 1-D model is used to describe the entire arterial system.

Equations A straightforward derivation of the 1-D model can be found in [17]. The resulting governing equations for continuity of mass and momentum are

$$\begin{cases} \dfrac{\partial A}{\partial t} + \dfrac{\partial Q}{\partial z} = 0, \\ \dfrac{\partial Q}{\partial t} + \dfrac{\partial}{\partial z}\left(\alpha \dfrac{Q^2}{A}\right) + \dfrac{A}{\rho_{\mathrm{f}}}\dfrac{\partial P}{\partial z} + K_r \dfrac{Q}{A} = 0, \end{cases} \tag{3}$$

where A is the area of the vessel, P is the mean pressure, Q is the volumetric flow rate, α is the Coriolis coefficient, and K_r is the friction coefficient accounting for fluid viscosity.

In order to close the problem an additional equation relating the averaged pressure with the other unknowns Q and A is needed. A complete mechanical model for the structure of the vessel wall is described in [1]. Here we consider only the elastic and viscoelastic contributions, as all the other terms are negligible in a cardiovascular setting, leading to the following pressure-area relation (see [18])

$$P - P_{\mathrm{ext}} = \beta\left(\sqrt{\frac{A}{A^0}} - 1\right) + \frac{\gamma}{A\sqrt{A}}\frac{\partial A}{\partial t}, \tag{4}$$

with

$$\beta := \sqrt{\frac{\pi}{A^0}}\frac{hE}{1-\nu^2}, \quad \gamma := \frac{T\tan\phi}{4\sqrt{\pi}}\frac{hE}{1-\nu^2},$$

where P_{ext} is the external pressure (i.e. the pressure of the tissues on the external wall), A^0 is the area of the cross-section of the vessel in the pre-stressed configuration, h is the wall thickness, E is the elastic Young modulus, ν is the Poisson coefficient, T is a characteristic time (usually taken equal to the systolic period), and ϕ is the so-called viscoelastic angle. Note that the viscoelastic term in (4) leads to an algebraic-differential equation which requires a special treatment when plugged into (3), as we show in the following paragraph.

Numerical approximation By inserting (4) into (3), after some manipulations, we get a system of differential equations that can be written in a classical conservative form as follows

$$\frac{\partial \boldsymbol{U}}{\partial t} + \frac{\partial \boldsymbol{F}(\boldsymbol{U})}{\partial z} + \boldsymbol{S}(\boldsymbol{U}) = 0, \tag{5}$$

where $\boldsymbol{U}$ are the conservative variables, $\boldsymbol{F}$ the corresponding fluxes, and $\boldsymbol{S}$ represents the source terms.

Following [1] we solve problem (5) by using an operator splitting technique, where the flow rate is split into two components such that $Q = \hat{Q} + \tilde{Q}$, where $\hat{Q}$ is the solution of the pure elastic problem and $\tilde{Q}$ is the viscoelastic correction. Let us consider the time interval $[t^n, t^{n+1}]$, for $n = 0, 1, 2, \ldots$, with $t^n = n\Delta t$, Δt being the time step:

1st step, elastic response: given $\boldsymbol{U}_h^n$, find $\hat{\boldsymbol{U}}_h^{n+1} = [A_h^{n+1}, \hat{Q}_h^{n+1}]^T \in \boldsymbol{\mathcal{V}}_h$ such that

$$\begin{aligned}(\hat{\boldsymbol{U}}_h^{n+1}, \varphi_h) = (\boldsymbol{U}_h^n, \varphi_h) + \\ \Delta t\left[\left(\boldsymbol{F}(\boldsymbol{U}_h^n), \frac{\partial \varphi_h}{\partial z}\right) - (\boldsymbol{S}(\boldsymbol{U}_h^n), \varphi_h)\right] - \\ \left(-\frac{\Delta t^2}{2}\frac{\partial \boldsymbol{F}(\boldsymbol{U}_h^n)}{\partial \boldsymbol{U}}\boldsymbol{\mathcal{H}}(\boldsymbol{U}_h^n), \frac{\partial \varphi_h}{\partial z}\right) + \\ \left(\frac{\Delta t^2}{2}\frac{\partial \boldsymbol{S}(\boldsymbol{U}_h^n)}{\partial \boldsymbol{U}}\boldsymbol{\mathcal{H}}(\boldsymbol{U}_h^n), \varphi_h\right), \quad \forall \varphi_h \in \boldsymbol{\mathcal{V}}_h\end{aligned}$$

where $\boldsymbol{U}_h$ is the discrete counterpart of $\boldsymbol{U}$, $\boldsymbol{\mathcal{V}}_h$ is the space of piecewise linear Finite Element (FE) functions, and

$$\boldsymbol{\mathcal{H}}(\boldsymbol{U}_h^n) := \frac{\partial \boldsymbol{F}(\boldsymbol{U}_h^n)}{\partial z} + \boldsymbol{S}(\boldsymbol{U}_h^n).$$

2nd step, viscoelastic correction: given $\hat{\boldsymbol{U}}_h^{n+1}$, find $\tilde{Q}_h^{n+1} \in \boldsymbol{\mathcal{V}}_h$ such that

$$\begin{aligned}\left(\frac{\tilde{Q}_h^{n+1}}{A_h^{n+1}}, \varphi_h\right) + \Delta t\left(\frac{\gamma}{\rho\left(A_h^{n+1}\right)^{3/2}}\frac{\partial \tilde{Q}_h^{n+1}}{\partial z}, \frac{\partial \varphi_h}{\partial z}\right) = \\ -\Delta t\left(\frac{\gamma}{\rho\left(A_h^{n+1}\right)^{3/2}}\frac{\partial \hat{Q}_h^{n+1}}{\partial z}, \frac{\partial \varphi_h}{\partial z}\right), \quad \forall \varphi_h \in \boldsymbol{\mathcal{V}}_h.\end{aligned}$$

The first step corresponds to an explicit second-order Taylor–Galerkin (TG) scheme, where we neglect the viscoelastic component of the wall. The problem is closed by imposing a suitable set of boundary and compatibility conditions on both sides of the 1-D segment. For the second step, we impose either homogeneous Dirichlet or homogeneous Neumann boundary conditions, depending from the

boundary conditions applied to the previous step. More details about the boundary conditions are given in [18].

On the one hand, the explicit nature of the TG scheme leads to a very fast and efficient solution of the numerical problem. However, on the other hand, it entails a strong limitation on the time step, that may be problematic when coupling with 3-D FSI models, as we will see in a forthcoming section.

0-D model

The peripheral 1-D arterial vessels are terminated with a three-element windkessel model (see Figure 1), which accounts for the cumulative effects of all distal vessels (small arteries, arterioles, and capillaries) beyond a terminal site.

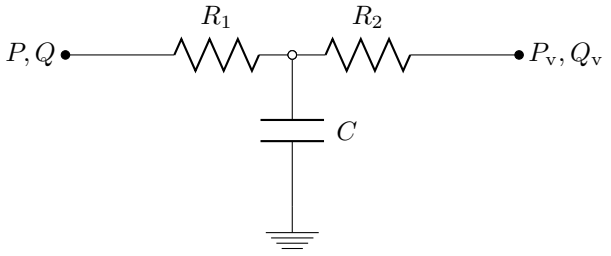

Figure 1 Three-element windkessel model.

The three-element windkessel model accounts for the proximal resistance R_1, the compliance C, and the distal resistance R_2 of the vascular network. The values of these parameters are given by *in vivo* measurements and reasonable assumptions (see [5]). This model leads to a differential relation between the the pressure and the flow in the time domain

$$\frac{\mathrm{d}P}{\mathrm{d}t} = -\frac{P}{CR_2} - \frac{R_1+R_2}{CR_2}Q - R_1\frac{\mathrm{d}Q}{\mathrm{d}t} + \frac{P_\mathrm{v}}{CR_2}, \quad (6)$$

where P and Q are the pressure and the flow rate at the terminal node of the 1-D segment, respectively, and $P_\mathrm{v} = 6666$ dyn/cm^2 [5 mmHg] is the prescribed venous pressure.

Numerical approximation Equation (6) can be solved for the pressure or for the flow rate. In the former case, by introducing the following approximation

$$\begin{cases} Q(t) \approx Q^n + \dfrac{Q^{n+1}-Q^n}{t^{n+1}-t^n}(t-t^n), \\ \dfrac{\mathrm{d}Q}{\mathrm{d}t} = \dfrac{Q^{n+1}-Q^n}{t^{n+1}-t^n} \end{cases}$$

we can integrate analytically (6), leading to an algebraic expression for the unknown pressure. The same approach holds when solving for the flow rate.

Geometrical multiscale algorithms

In this section we briefly describe the techniques we develop to couple the models introduced in the previous section.

Coupling the fluid

In a geometrical multiscale setting, where the models are defined in different geometrical spaces (e.g., 0-D, 1-D, 3-D, etc.), the problem at the coupling interfaces can be formulated in a general way only by writing the conservation equation in terms of averaged/integrated quantities. In particular, for a generic fluid coupling interface Γ_f, we select

$$Q = \int_\Gamma \boldsymbol{u}\cdot\boldsymbol{n}\,\mathrm{d}\Gamma_\mathrm{f} \quad \text{and} \quad \Sigma = \frac{1}{|\Gamma_\mathrm{f}|}\int_{\Gamma_\mathrm{f}} (\boldsymbol{\sigma}\cdot\boldsymbol{n})\cdot\boldsymbol{n}\,\mathrm{d}\Gamma_\mathrm{f},$$

where Q is the volumetric flow rate and Σ is the average of the normal component of the traction vector, hereafter referred to as the *coupling stress*. Specifically, we choose to consider that $(\boldsymbol{\sigma}\cdot\boldsymbol{n})\cdot\boldsymbol{n}$ is constant over Γ_f in order to close the problem. This choice leads to the following conservation equations for the problem at the coupling interfaces:

$$\forall c = 1,\dots,\mathcal{C}\ : \quad \begin{cases} \displaystyle\sum_{m=1}^{\mathcal{M}_c} Q_{c,m} = 0, \\ \Sigma_{c,1} = \Sigma_{c,m}, \quad \forall m = 2,\dots,\mathcal{M}_c, \end{cases} \quad (7)$$

where $\mathcal{C}$ is the total number of coupling interfaces of the network of model and $\mathcal{M}_c$ is the number of models coupled by the c-th coupling interface (see Figure 2). To satisfy the set of equations (7), different coupling strategies can be used, corresponding to the imposition of different quantities on the boundaries. In other words, we can set up each subproblem with different combinations of boundary data over the coupling interfaces. Some examples are provided in [13].

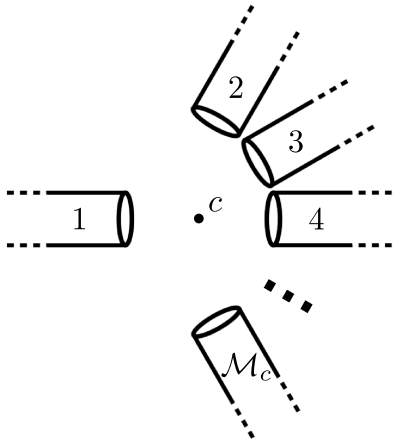

Figure 2 General configuration for the c-th coupling between $\mathcal{M}_c$ models.

Coupling the solid

The coupling between the solid parts of the models can be achieved with a similar approach, i.e., by imposing the continuity of the area over the coupling interfaces. However, from the practical viewpoint, the imposition of the area on the 1-D model is equivalent to impose a pressure, and this is already done by coupling the fluid problem. Moreover, due to the sub-critical nature of the flow field (see [1]), the 1-D model can receive just one physical quantity on each side of the 1-D segment, that is already a fluid quantity. Nevertheless, it is possible to impose on the 3-D solid ring the value of a given area, for example, by a 1-D model. Investigations in this direction are subject of future works. The results presented in this paper are obtained by clamping the solid interface of the 3-D FSI model. Even if this condition is not physical, it is necessary for the well-posedness of the problem, which can be solved only by removing the rigid modes from the 3-D FSI model.

Numerical approach

Let $\boldsymbol{\lambda}$ be the global vector of coupling variables. The problem at the coupling interfaces is solved by using a classical non-linear Richardson strategy

$$\boldsymbol{\lambda}^{k+1} = \boldsymbol{\lambda}^{k} + \delta\boldsymbol{\lambda}^{k},$$

until convergence to a suitable tolerance has been achieved. In order to devise a convergent methodology, we make use of the Newton method

$$J(\boldsymbol{\lambda}^{k})\delta\boldsymbol{\lambda}^{k} = -\mathcal{R}(\boldsymbol{\lambda}^{k}),$$

which requires the computation of the exact Jacobian matrix $J(\boldsymbol{\lambda}^{k})$ at each iteration. Each coefficient of the Jacobian matrix corresponds to the variation of a boundary value due to the variation of a coupling quantity on the same model. Therefore, from the computational point of view, each coefficient requires the solution of the tangent problem associated to the corresponding model (see [13] for more details on the computation and assembling of the Jacobian matrix). This approach is very expensive, especially when dealing with many 3-D FSI boundary interfaces. Moreover the Jacobian matrix should be updated at each iteration. In view of these considerations, we use the Newton method only at the very first iteration, to initialize the Jacobian matrix. Then we update the matrix at each iteration through the Broyden method

$$J(\boldsymbol{\lambda}^{k}) = J(\boldsymbol{\lambda}^{k-1}) + \frac{\left(\mathcal{R}(\boldsymbol{\lambda}^{k}) - \mathcal{R}(\boldsymbol{\lambda}^{k-1})\right)\left(\delta\boldsymbol{\lambda}^{k-1}\right)^{T}}{(\delta\boldsymbol{\lambda}^{k-1})^{T}\delta\boldsymbol{\lambda}^{k-1}} - \frac{\left(J(\boldsymbol{\lambda}^{k-1})\delta\boldsymbol{\lambda}^{k-1}\right)\left(\delta\boldsymbol{\lambda}^{k-1}\right)^{T}}{(\delta\boldsymbol{\lambda}^{k-1})^{T}\delta\boldsymbol{\lambda}^{k-1}},$$

which does not require the solution of any tangent problem.

A two-level time step technique for coupling 1-D and 3-D FSI models

As anticipated before, the explicit second order TG scheme entails a strong time step limitation due to the low value of the Courant–Friedrichs–Lewy (CFL) condition, equal to $\sqrt{3}/3$. In particular, under physiological conditions this leads to a maximum time step of about 1e-5 s, that is around one hundred times smaller that the one typically used for 3-D FSI simulations. Indeed, 3-D FSI models are very expensive from the computational viewpoint and for this reason we aim to solve them as few times as possible, i.e., using a very large time step.

In order to satisfy the 1-D CFL condition without reducing the 3-D FSI time step, we devise a two-level time step technique (see Figure 3) where

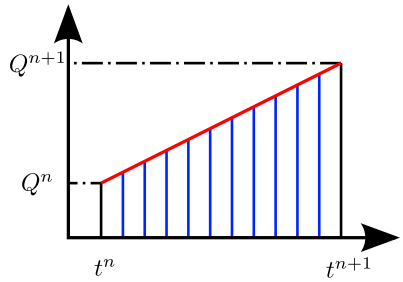

Figure 3 Two-level time step technique scheme: between the global time step $\Delta t = t^{n+1} - t^{n}$, some local time steps (in blue) are performed in the 1-D models.

- the inner time step meets the 1-D CFL requirements and it is used just by the 1-D models;
- the outer time step is used for the 3-D FSI model and for the strong coupling between the models, i.e., (7) is satisfied just at this level.

Note that in order to perform the inner time steps, we need to interpolate the values of the coupling conditions between t^{n} and t^{n+1}.

The resulting scheme is robust from the computational point of view, however two problems may arise. First of all, we need to find a different strategy for the computation of the Jacobian coefficients, since the analytical formulation of the tangent problem is too complex due to the recursion of the problem. To address this issue we use two different techniques: a finite difference approximation and an approximated formulation of the tangent problem. In both cases we end up with convergent inexact-Newton schemes. Another issue regards the possible presence of numerical reflections at the coupling interfaces, due to the fact that (7) are satisfied just at the outer time step. Nevertheless, investigations in this direction show that these reflections are strongly related to the size of the wavelength. In particular under physiological conditions the wavelengths are long and the numerical reflection are negligible.

More details and investigations about the two-level time step technique and these issues are given in [18].

Results

In this section we show some numerical results and applications of the methodology discussed in the previous sections.

1-D modeling of the human arterial network

First of all, we validate our methodology by using the arterial network provided in [5, Figure 2 and Table 2]. This model is composed by 103 elements (4 coronary, 24 aortic, 51 cerebral, 10 in the arms, and 14 in the legs) and includes all the parameters required to describe the true physiological flow, such as the narrowing of the area, the viscoelastic response of the arterial wall, and the terminals, which are modeled as 0-D windkessel elements. The resulting coupled problem is composed of 255 interface variables. Even if the number is relatively small, it represents the implicit coupling of 150 (103 1-D plus 47 0-D) non-linear problems, in a complex network topology (that includes bifurcations and closed loops), hence the solution is not trivial.

In Figure 4 we present the result of the last of six cardiac cycles, when the periodic regime has been reached. We can observe that our results follow the ones given in [5, Figure 4], even if some differences are present, due to the different model for the viscoelastic part of the arterial wall and to the different heart flow rate time profile. Regarding the number of iterations of the coupling algorithm we tested different methods in presence of the two-level time step technique (in view of the coupling with 3-D FSI models), using an outer time step of 0.001 s, which is the typical one for 3-D FSI simulations. The results are shown in Figure 5, where we observe that the Broyden strategy leads to a reduction factor of five with respect to the inexact-Newton method. Note that there are no significant differences between the cases with and without the viscoelastic term, even if it adds some additional non-linearities to the problem.

1-D arterial network with 3-D FSI aorta

In this paragraph we present some preliminary results about the coupling of the full 1-D network with a 3-D FSI aorta. The layout of the model is shown in Figure 6. To set up the model, first of all we identify the position of the 7 coupling interfaces of the 3-D aorta in the 1-D arterial network. Then, we perform a cut of the 1-D segments at those positions, such that we match the original length of the 1-D arterial network. Finally, we also change the proximal diameter in those segments in order to match the one of the corresponding 3-D FSI interfaces. On the one hand, this procedure may seem somehow arbitrary, in the sense that there is not a unique technique to identify the cutting sections, nor the correct length of the 1-D segments. However, on the other hand, this arbitrariness should not affect the results, as the values of the averaged/integrated quantities (volumetric flow rate and normal stress) is not affected by small geometrical changes.

The mesh of the fluid part of the aorta consists of 271,970 tetrahedral elements with 54,131 vertices, while the solid part is made of 108,720 tetrahedral elements with 35,944 vertices. All simulations were performed on three computational nodes with eight cores each of the Intel Nehalem cluster *Antares* at the EPFL. The simulation of one heartbeat takes approximately 52 hours of wall-clock time. In Figure 7 we show a detailed view of the velocity field inside the 3-D FSI aorta, while regarding the number of iterations in Figure 8 we can observe that there is no significant difference between the full 1-D arterial network case and the coupled 1-D plus 3-D FSI aorta one. Note that the two green peaks correspond to a restart of the simulation where, at the present time, we lose the information about the previous Jacobian matrix; in the future we plan to store the last Jacobian matrix for the next restart, in order to solve this small issue. For the full 1-D network a restart is not needed due to the small computational cost.

Sensitivity analysis of the external wall Robin boundary condition for the 3-D FSI model

From the modeling point of view, one critical aspect to get physiological results in the 3-D FSI aorta is the tuning of the boundary condition on the solid external wall. The influence of external tissues and organs tethering and constraining the movement of blood vessels is of critical importance when simulating 3-D FSI problems in the arterial system. Obviously, it is currently unfeasible to model the detailed multi-contact relations between the aortic system and the other tissues. In [19] the authors propose to handle the external tissue support on the outer arterial wall by enforcing a Robin boundary condition which models the elastic and viscoelastic response of the tissue. For the sake of simplicity, we start our analysis by neglecting the viscoelastic component. Therefore on the solid wall of the 3-D FSI problem we impose

$$\mathbf{\Pi} \cdot \mathbf{n}_\mathrm{s} + k_s \cdot \mathbf{d}_\mathrm{s} + P_\mathrm{wall} \cdot \mathbf{n}_\mathrm{s} = 0, \quad \text{on } \Gamma_\mathrm{wall},$$

where k_s is an empiric elastic coefficient. Then we set up different test cases of the same problem. In particular, we identify three main regions in the aortic arch and we select different sets of values for the elastic coefficient k_s (see Table 1). The results at the ascending and thoracic aorta coupling interfaces are shown in Figures 9 and 10, respectively. As we can see from the images, the first three sets of coefficients (the smallest ones, including also a Neumann case) lead to unphysiological results. Removing those cases from the graphs we end up with very similar results (see the second row in Figures 9 and 10), where strong variations of the elastic coefficient does not produce sensible variations of the main quantities. Moreover, these latest results are in a physiological range and comparable to the ones obtained with the full 1-D arterial network. Further tests including the viscoelastic term in the Robin boundary condition are subject of future works.

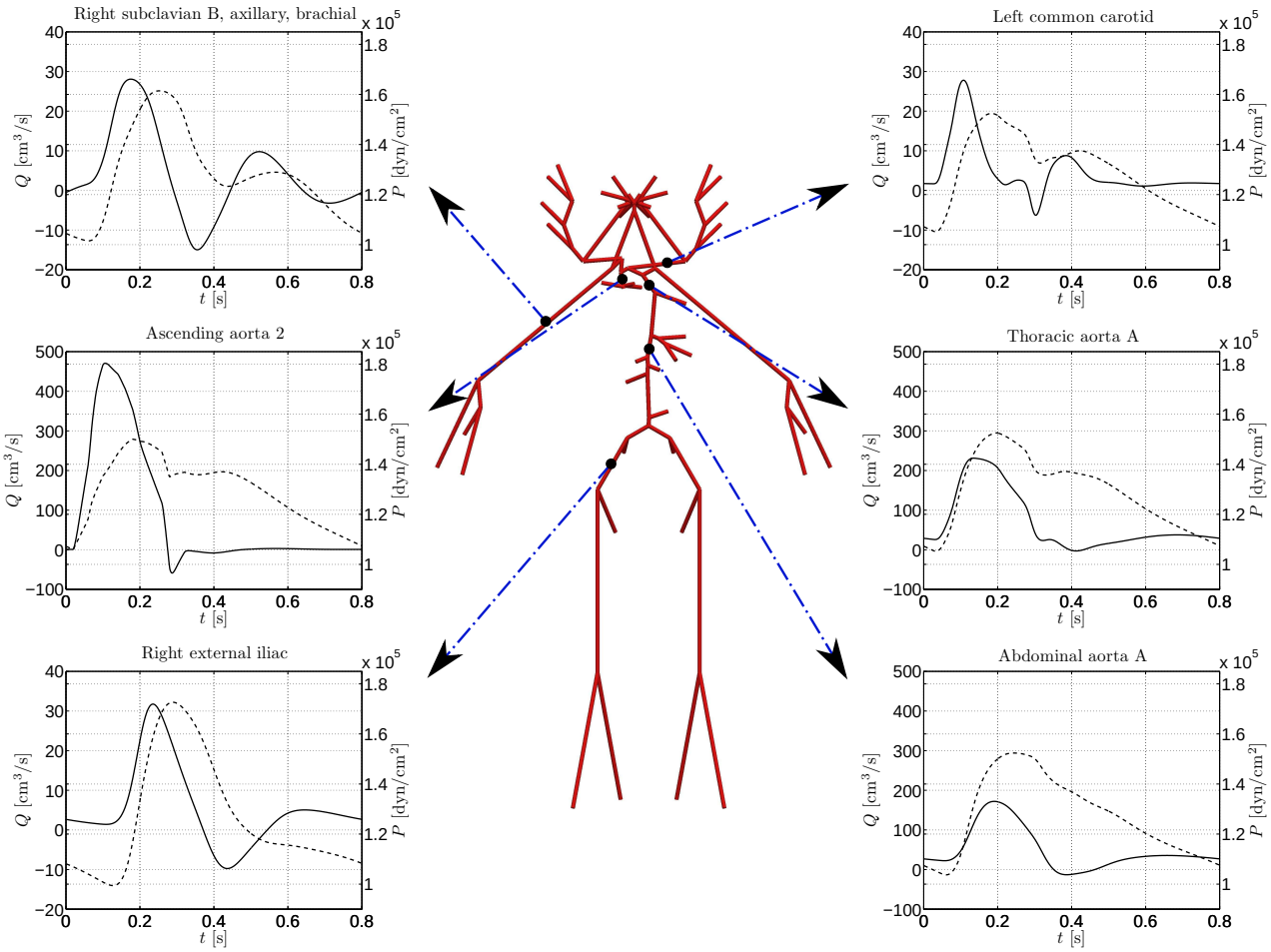

Figure 4 Periodic flow rate (solid line) and pressure (dashed line) results in six different arterial segments. Positioning of 1-D network elements is purely visual.

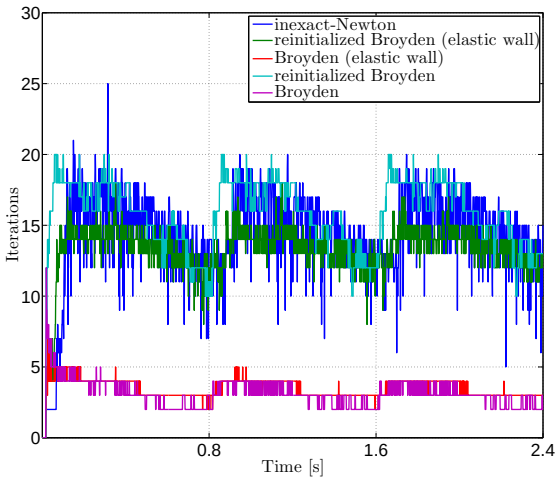

Figure 5 Comparison, in terms of number of iterations, of different algorithms for the coupling of the full 1-D network. The first three heart beats are shown. Note that in the Broyden method $J(\lambda^0)$ is the Jacobian matrix of the previous time step, while in the reinitialized version, it is recomputed using the inexact-Newton method.

Conclusions

In the present work, a geometrical multiscale framework for modeling the human cardiovascular system has been presented. The main ingredients of the framework are (i) a complete set of models for describing each compartment of the arterial network with a proper level of detail (0-D, 1-D, and 3-D), and (ii) a general and robust coupling algorithm to assemble the heterogeneous models into one large geometrical multiscale problem.

We show that our geometrical multiscale framework is able to assemble and solve complex problems, including networks of more that 100 elements, with a reasonable computational cost. Moreover, we also demonstrate that the resulting geometrical multiscale model provides physiological results, comparable with the ones of Reymond et al. [5].

Finally we also show some preliminary results of heterogeneous networks, coupling a 3-D FSI aorta with a full 1-D arterial tree. For this challenging application we show that correctly tuning the value of the external wall Robin boundary condition on the 3-D FSI problem we obtain physiological results, comparable to the ones of the full 1-D arterial network. Further test and investigations on this field are subject of future works.

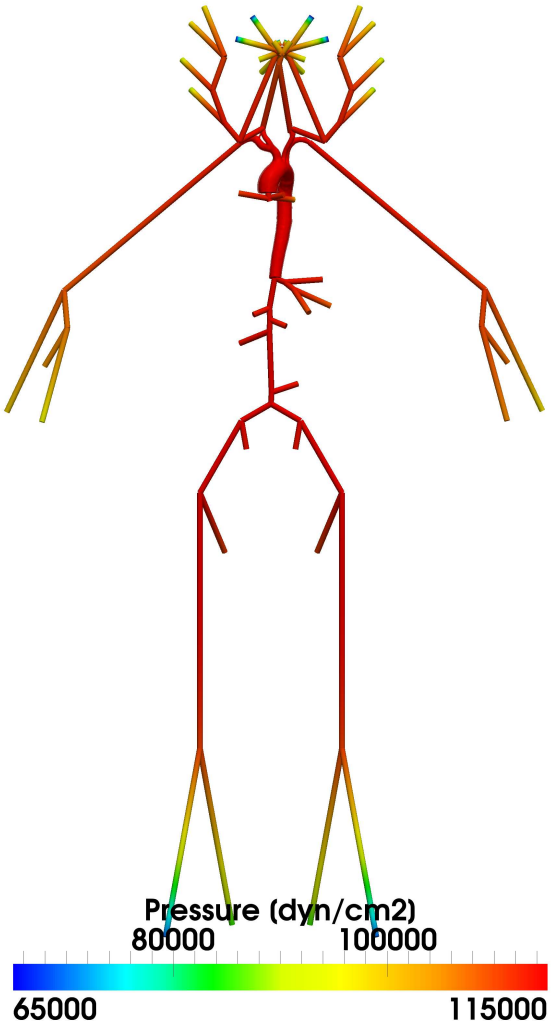

Figure 6 A global view of the 1-D arterial network coupled with the 3-D FSI aorta at the beginning of the 3rd systole. Positioning of 1-D network elements is purely visual.

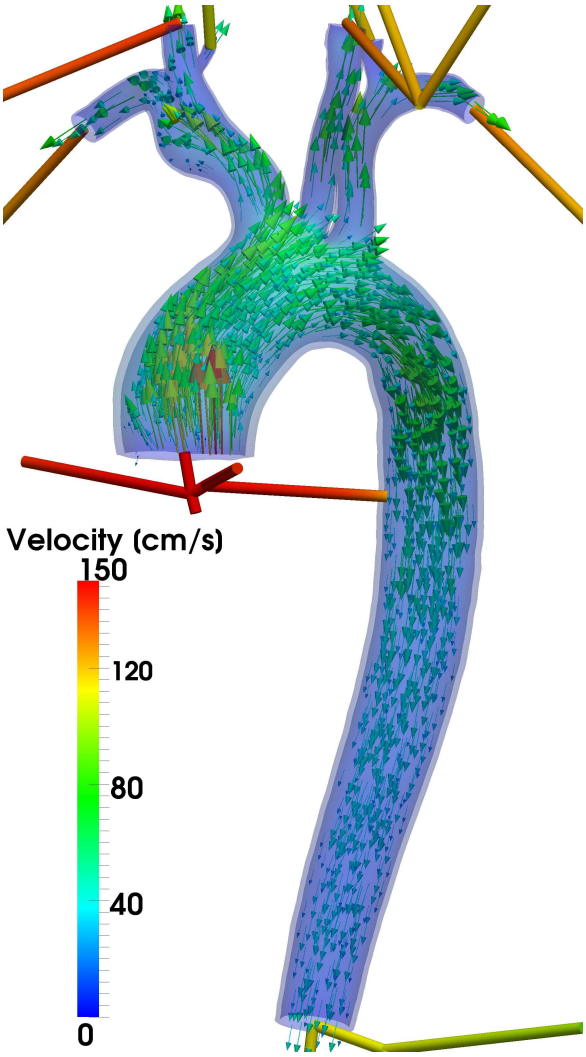

Figure 7 A view of the 3-D aortic arc velocity field during the systolic peak of the 3rd heart beat. The color of the 1-D segments refers to the pressure field (blue: 65000 dyn/cm^2, red: 115000 dyn/cm^2). Positioning of 1-D network elements is purely visual.

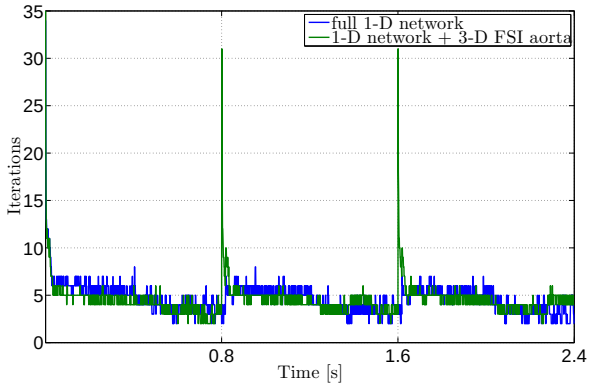

Figure 8 Comparison, in terms of number of Broyden iterations, between the full 1-D arterial network and the coupled 3-D FSI aorta plus 1-D network. The first three heart beats are shown.

Acknowledgements

A.C.I. Malossi and S. Deparis acknowledge the European Research Council Advanced Grant “Mathcard, Mathematical Modelling and Simulation of the Cardiovascular System", Project ERC-2008-AdG 227058 and the the Swiss Platform for High-Performance and High-Productivity Computing (HP2C). P.J. Blanco acknowledges the support of the Brazilian agencies CNPq and FAPERJ. We acknowledge the support of the Swiss-Brazilian Fund, Project BJRP 011010 (N 590002/2010-4) We also thank Prof. L. Formaggia of MOX/Politecnico di Milano for his precious support on the development of the 1-D model. All of the numerical results presented in this paper have been computed using the `LifeV` library (`www.lifev.org`). `LifeV` is the joint collaboration between four institutions: École Polytechnique Fédérale de Lausanne (CMCS) in Switzerland, Politecnico di Milano (MOX) in Italy, INRIA (REO, ESTIME) in France, and Emory University (Sc. Comp) in the USA.

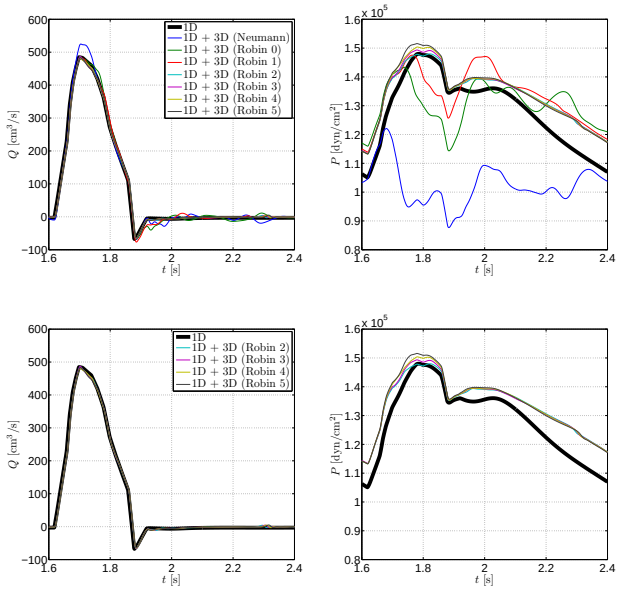

Figure 9 Comparison between the result at the ascending aorta of the full 1-D arterial network (black thick line) with the ones of the 1-D arterial network coupled with the 3-D FSI aorta in presence of different wall conditions. The first line shows the results of all the tested cases, while the second line shows just a subset of them.

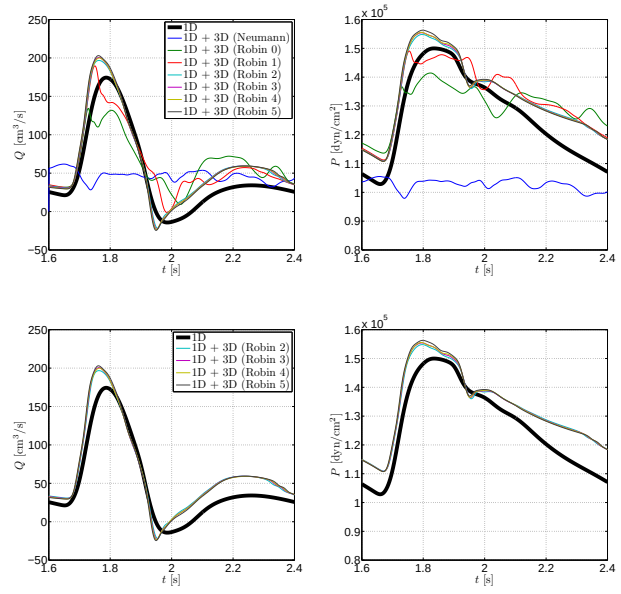

Figure 10 Comparison between the result at the thoracic aorta of the full 1-D arterial network (black thick line) with the ones of the 1-D arterial network coupled with the 3-D FSI aorta in presence of different wall conditions. The first line shows the results of all the tested cases, while the second line shows just a subset of them.

Table 1 Sets of values for the elastic coefficient k_s of the 3-D FSI aorta external wall Robin boundary condition. See the figure below to identify the three regions (Top, Center, and Bottom).

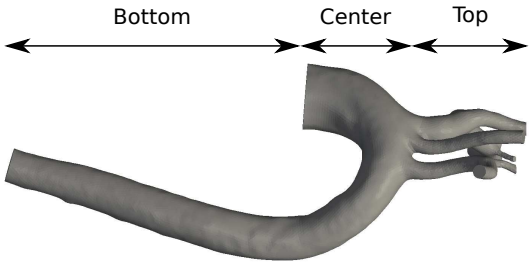

	k_s		
Wall condition	Top	Center	Bottom
Neumann	0	0	0
Robin 0	30000	10000	19000
Robin 1	40000	15000	25000
Robin 2	55000	20000	35000
Robin 3	80000	30000	50000
Robin 4	95000	40000	65000
Robin 5	110000	50000	80000

References

[1] L. Formaggia, D. Lamponi, and A. Quarteroni. One-dimensional models for blood flow in arteries. *J. Eng. Math.*, 47(3–4):251–276, 2003.

[2] S.J. Sherwin, V. Franke, J. Peiró, and K. Parker. One-dimensional modelling of a vascular network in space-time variables. *J. Eng. Math.*, 47(3):217–250, 2003.

[3] L. Formaggia, D. Lamponi, M. Tuveri, and A. Veneziani. Numerical modeling of 1D arterial networks coupled with a lumped parameters description of the heart. *Comput. Methods Biomech. Biomed. Engin.*, 9(5):273–288, 2006.

[4] S. Čanić, C.J. Hartley, D. Rosenstrauch, J. Tambača, G. Guidoboni, and A. Mikelić. Blood flow in compliant arteries: an effective viscoelastic reduced model, numeric and experimental validation. *Ann. Biomed. Eng.*, 34(4):575–592, 2006.

[5] P. Reymond, F. Merenda, F. Perren, D. Rüfenacht, and N. Stergiopulos. Validation of a one-dimensional model of the systemic arterial tree. *Am. J. Physiol. Heart Circ. Physiol.*, 297(1):H208–H222, 2009.

[6] P.J. Blanco, R.A. Feijóo, and S.A. Urquiza. A unified variational approach for coupling 3D–1D models and its blood flow applications. *Comp. Meth. Appl. Mech. Engrg.*, 196(41–44):4391–4410, 2007.

[7] L. Formaggia, A. Quarteroni, and A. Veneziani. *Cardiovascular Mathematics*, volume 1 of *Modeling, Simulation and Applications*. Springer, Milan, 2009.

[8] L. Formaggia, J.F. Gerbeau, F. Nobile, and A. Quar-

teroni. Numerical treatment of defective boundary conditions for the Navier–Stokes equations. *SIAM J. Numer. Anal.*, 40(1):376–401, 2002.

[9] A. Veneziani and C. Vergara. Flow rate defective boundary conditions in haemodynamics simulations. *Int. J. Num. Meth. Fluids*, 47(8–9):803–816, 2005.

[10] Paolo Crosetto, Philippe Reymond, Simone Deparis, Dimitrios Kontaxakis, Nikolaos Stergiopulos, and Alfio Quarteroni. Fluid-structure interaction simulation of aortic blood flow. *Computers & Fluids*, 43(1):46–57, 2011. Symposium on High Accuracy Flow Simulations. Special Issue Dedicated to Prof. Michel Deville.

[11] L. Formaggia, J.F. Gerbeau, F. Nobile, and A. Quarteroni. On the coupling of 3D and 1D Navier–Stokes equations for flow problems in compliant vessels. *Comp. Meth. Appl. Mech. Engrg.*, 191(6–7):561–582, 2001.

[12] T. Passerini, M. de Luca, L. Formaggia, A. Quarteroni, and A. Veneziani. A 3D/1D geometrical multiscale model of cerebral vasculature. *J. Eng. Math.*, 64(4):319–330, 2009.

[13] A.C.I. Malossi, P.J. Blanco, S. Deparis, and A. Quarteroni. Algorithms for the partitioned solution of weakly coupled fluid models for cardiovascular flows. *Int. J. Num. Meth. Biomed. Engng.*, 2011.

[14] F. Nobile. *Numerical approximation of fluid-structure interaction problems with application to haemodynamics*. PhD thesis, École Polytechnique Fédérale de Lausanne, 2001.

[15] P. Crosetto, S. Deparis, G. Fourestey, and A. Quarteroni. Parallel algorithms for fluid-structure interaction problems in haemodynamics. *SIAM J. Sci. Comput.*, 33(4):1598–1622, 2011.

[16] E. Burman, M.A. Fernández, and P. Hansbo. Continuous interior penalty finite element method for Oseen's equations. *SIAM J. Numer. Anal.*, 44(3):1248–1274, 2006.

[17] A. Quarteroni and L. Formaggia. *Modelling of Living Systems*, chapter Mathematical Modelling and Numerical Simulation of the Cardiovascular System. Handbook of Numerical Analysis Series. Elsevier, 2003.

[18] A.C.I. Malossi, P.J. Blanco, and S. Deparis. A two-level time step technique for the partitioned solution of one-dimensional arterial networks. In preparation, 2011.

[19] P. Moireau, N. Xiao, M. Astorino, C.A. Figueroa, D. Chapelle, C.-A. Taylor, and J.-F. Gerbeau. External tissue support and fluid-structure simulation in blood flows. *Biomech. Model. Mechanobiol.*, 2011.